Quantitative Structure–Activity Relationships/Comparative Molecular Field Analysis (QSAR/CoMFA) for Receptor-Binding Properties of Halogenated Estradiol Derivatives

Tsvetan G. Gantchev, Hasrat Ali, and Johan E. van Lier*

MRC Group in the Radiation Sciences, Faculty of Medicine, University of Sherbrooke, Sherbrooke, Québec, Canada J1H 5N4

Received May 20, 1994[⊗]

The 3-D quantitative structure–activity relationships/comparative molecular field analysis (QSAR/CoMFA) paradigm, which considers the primary importance of the molecular fields in biological recognition, is now widely used to analyze and predict receptor-binding properties of various ligands. CoMFA was applied to build 3-D QSAR models of substituted estradiol–receptor interactions, employing 3-D molecular databases of more than 40 molecules. Ligands included the 17α-ethynyl- and isomeric 17α(20*E*/*Z*)-(iodovinyl)estradiols and their 7α-, 11β-, and 12β-methyl (-methoxy) and -ethyl (-ethoxy) derivatives as well as selected 2- and 4-halogenated analogs. The influence of different CoMFA descriptors was studied in order to achieve the highest possible cross-validated r^2, as derived from partial least-squares calculations. Special emphasis was put on the analysis of the nature of H-bonding (donor/acceptor) interactions. The model with the best predictive performance ($r^2 = 0.895$) was used to visualize steric and electrostatic features of the QSAR (standard deviation*coefficient contour maps) and to predict receptor-binding affinities (RBA) of substituted estradiols other than those included in the original database. Twenty-seven test molecules were selected, including five which had previously been reported by other investigators. For the latter, a very good correlation with literature RBA values was obtained, which together with the high cross-validated r^2 provides evidence for the high predictive capacity of the model. Among the unknown structures, the model suggests several new substitutions to derive at reasonable affinity ligands for the estrogen receptor.

Introduction

The biological action of steroid hormones and their primary interactions with receptor proteins have been topics of much interest over the years. Particularly elucidation of the structural requirements which facilitate binding of the steroid molecules to their receptors has actively been persued as a means to develop novel therapeutic and diagnostic agents. However, the lack of resolved crystallographic structures of most of the cytoplasmic steroid receptors has hampered a complete understanding of the underlying physicochemical mechanisms of steroid hormone–receptor interactions. On the basis of the general assumption that noncovalent forces dominate receptor–drug interactions, and that these forces can be described in terms of steric and electrostatic effects, new approaches have been developed to compensate for the absence of detailed protein structure information and to correlate drug structures to biological activities. The method of Cramer et al.[1a] provides 3-D quantitative structure–activity relationships (QSAR) using comparative molecular field analysis (CoMFA). The procedure involves partial least-squares (PLS) statistics to compute separately the contributions of steric (shape) and electrostatic (electronic) molecular field lattices, providing physical parameters which can than be correlated to specific biological properties of the molecules.[1b,c] In their pioneering study, Cramer et al.[1a] applied this methodology to examine and predict biological properties of steroid analogs toward testosterone- and corticosteroid-binding globulins. A more recent study uses the QSAR/CoMFA technique to elucidate progestin and androgen receptor-binding properties of substituted steroids.[1d] This approach is now widely used to predict binding affinities of modified ligands to various receptor proteins and enzymes.[2]

Halogenated estrogens have been extensively studied as radiopharmaceuticals for receptor imaging in the management of endocrine cancers.[3] In addition to a high receptor-binding affinity, design of such agents requires a rapid labeling step to introduce a short-lived radioisotope as the final structural modification. Among the different procedures to functionalize the parent estradiol molecule, radioiodination at the 16α-[4] or 17α-vinyl-positions[5] was found particularly promising. The resulting derivatives exhibit good receptor-binding properties and *in vivo* stability, and several analogs were shown to exhibit target tissue selectivity. Since the main metabolic pathways of estrogens involve modifications of the A- and D-rings of the steroid backbone, appropriate substitutions at these sites can further improve uptake by estrogen receptor-rich tissues.[6] Thus, introduction of fluorine atoms at the 2- or 4-positions on the steroid A-ring was shown to alter target tissue selectivity of the radiolabeled ligand.[7] On the other hand, substitutions onto the 7α- and 11β-positions on the steroidal B- and C-rings are known to diminish nonspecific binding and increase the stability of the steroid–receptor complex, resulting in favorable biodistribution of the ligand for imaging purposes.[8,9]

In view of the large amount of structure–activity information available for halogenated estrogens and their receptor-binding properties, it is now possible to build a molecular database and derive a QSAR/CoMFA model for 3-D space mapping of the interactions of

⊗ Abstract published in *Advance ACS Abstracts*, October 15, 1994.

0022-2623/94/1837-4164$04.50/0 © 1994 American Chemical Society

estradiol derivatives with the estrogen receptor (ER). Furthermore, correlating receptor-binding properties of modified steroids in terms of QSAR/CoMF analysis allows us to predict the biological properties of unknown analogs. The estradiol (E_2) derivatives used in the present study were selected to represent a basic set of over 40 molecules covering characteristic steroid substitution patterns, including the effect of (i) stereoselectivity in the case of the 17α-ethynyl (EE_2) and isomeric 17α(20*E*/*Z*)-iodovinyl (IVE_2) substituents, (ii) electron-withdrawing groups and steric bulk (F, Cl, Br, and I atoms) at 2-, 4-, and/or 17α(20*E*/*Z*)-positions, and (iii) electron-donating groups (CH_3O and C_2H_5O) and neutral groups (H_3C and C_2H_5) at 11β-, 12β-, and 7α-positions of the steroid skeleton. To obtain 3-D structures and electronic charge distributions, semiempirical molecular orbital computations were employed using MOPAC software (MNDO parametrization). The resultant steric and electronic properties of the computed molecules were analyzed with the graphics, geometry, and molecular mechanics tools of the SYBYL graphics interface (Tripos Assoc.). The molecular parameters were then combined with the known relative receptor-binding affinities (RBA) of the steroid derivatives to build the corresponding QSAR tables. CoMFA was performed using the PLS method, as included in the SYBYL/QSAR module.

Chemistry and Biological Data

The main set of estradiol derivatives which we used to build the QSAR/CoMFA model consists of 40 molecules, previously synthesized in our laboratory (Figure 1). They include a series derived from 17α-ethynylestradiol, A-ring-fluorinated estradiols,[7a] 11β- and 7α-substituted analogs,[5a,b] and a group of molecules featuring 17α-chloroethynyl or 17α-chlorovinyl substituents[10] (**1**–**40**). Their RBA for the ER were used as explicit biological data (column) in the QSAR tables. All RBA values were obtained under identical experimental conditions, using a competitive binding assay with [^{3}H]-estradiol.[11] Initial CoMFA training runs with these 40 estradiol derivatives indicated that the QSAR model was sensitive to electrostatic but not steric interactions about the A-ring. Therefore, four additional molecules were added to the database, including 2-iodo(bromo)- and 4-iodo(bromo)-substituted estradiols (**41**–**44**) (Figure 1). Only for these latter molecules RBA values were taken from data reported by others.[12] The resulting database of 44 molecules was employed to derive at the final QSAR/CoMFA model, which was used to analyze ER-binding properties and predict RBA values of estradiol derivatives not included in the database. The structures of these selected "unknowns" are shown in Figure 2. They include five test compounds (**45**–**48** and **51**) of which the RBA values are reported in the literature,[9,13] allowing us to judge the predictive capability of the model. The remaining molecules are estradiol derivatives which have not previously been reported, providing an example of how the model can be used for practical purposes.

Computational Methods

3-D Molecular Databases. All molecular modeling and CoMFA analyses were performed using SYBYL (versions 5.5 and 6.01)[14a] on IBM RISC 6000 UNIX workstations. Because of the relative rigidity of the steroid nucleus, the molecular structures of the estradiol derivatives were build starting from the unsubstituted estradiol (E_2). The atomic coordinates of E_2 were retrieved from the Cambridge Structural Database.[15] Low-energy conformations were determined by molecular mechanics with systematic search in the torsional space (MAXIMIN2 and SEARCH options of SYBYL) employing unmodified TRIPOS molecular mechanics force field. The resulting interatomic coordinates were used for computing the final molecular structures by means of semiempirical molecular orbital computations by MOPAC (versions 5.5–6.0) applying MNDO (modified neglect of diatomic overlap) Hamiltonian.[16] These were performed by full geometry optimization (all bonds, all angles), and the output options included bond order analysis, $\pi-\sigma$ compositions, and Mulliken atomic charge population.[17] Partial molecular charges of one molecular database were also computed using the empirical Gasteiger–Hückel method,[18] and the results were compared with those obtained by MOPAC.

3-D QSAR Studies by the CoMFA Method. CoMFA was performed with the QSAR module of SYBYL. Typically, steric (Lennard–Jones) and electrostatic (columbic) potentials were sampled for a grid of points in space around molecules and evaluated at lattice intersections of the grid with a 1 or 2 Å step size, a sp^3 hybridized carbon atom probe, and hydrogen or oxygen carrying formal charges of 1.0 and −1.0, respectively. The CoMFA lattice dimensions were 20 × 20 × 20 Å (x, y, z = −10–+10 Å) with 9261 points for a grid step of 1 Å. This grid region overlapped all entered molecules (aligned in the database) and extended beyond their van der Waals envelopes by at least 3–4 Å along all axes. A smaller region size and/or a greater grid step, as a rule, resulted in lower predictive capability of the model. The cutoff value for both steric and electrostatic interactions was set by the SYBYL default (30 kcal/mol). Several molecular alignment rules were tested during this study: field-fit minimization; restricted field-fit minimization with imposed A-, B-, C-, and D-ring carbon atom constraints; and root mean square (rms) fit of the backbone carbon atoms from the A-, B-, and C-rings of the steroid. The linear QSAR expressions from CoMFA computations were derived by the PLS analysis algorithm of SYBYL, in conjunction with the cross-validation. These calculations provided the optimal number of components required for a model with the best predictive properties, as indicated by the highest correlation (predictive r^2) values.[1a] PLS analyses with the descriptors obtained from cross-validated runs were used to afford conventional r^2 values and verify "robustness" of the CoMFA (bootstrapping). For most computations, the predictive RBA values were cross-validated using 40 cross-validation groups. Thus, each compound was predicted from a model that used all other compounds. Minimum σ values in field calculations were set to 2 throughout this study. Under these conditions, the computational index (UNIX 6000 RISC IBM computers) for cross-validated runs was as high as (20–30) × 10^6.

Results

Molecular Structures. Figure 3 shows superimposed energy-minimized structures of EE_2 and 20*E*/*Z*-IVE_2 (Figure 3a) and their 7α-Me-2(4)-F (Figure 3b) and 11β-OMe(OC_2H_5) (Figure 3c) derivatives, together with E_2 as template, obtained from MNDO computations. Introduction of the different substituents onto the E_2 template results in subtle perturbations of the overall conformation of the steroid skeleton. The most pronounced structure deviations occur upon 17α-substitutions about the D-ring and include a small displacement of the 17β-OH group, the 15- and 16-hydrogens, and the spatial orientation of the methyl at C-13. Substitutions at the 7α- and 11β-positions influence slightly the conformation of the B- and C-rings. Substituents at the 2(4)-positions did not result in any distortion of the steroid backbone (Figure 3b).

In the case of the 17α-vinylestradiols (VE_2), two local energy minima were obtained such that the vinyl side-

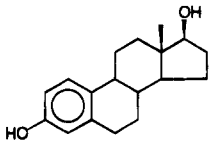

1

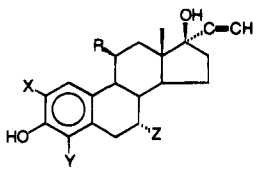

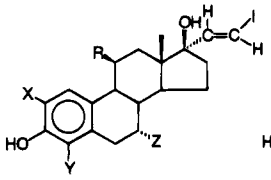

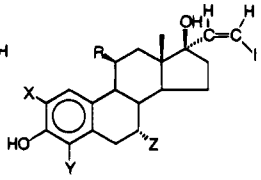

X	Y	Z	R			
H	H	H	H	2	3	4
F	H	H	H	5	6	7
H	F	H	H	8	9	10
H	H	H	OCH_3	11	12	13
F	H	H	OCH_3	14	15	16
H	F	H	OCH_3	17	18	19
H	H	H	OC_2H_5	20	21	–
H	H	CH_3	H	22	23	24
F	H	CH_3	H	25	26	27
H	F	CH_3	H	28	29	30

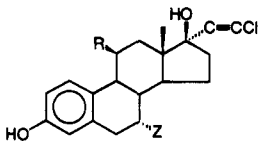

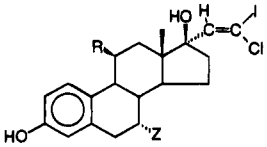

Z	R		
H	H	31	32
H	OCH_3	33	34
H	OC_2H_5	35	36
CH_3	H	37	38

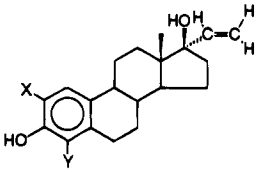

X	Y	
F	H	39
H	F	40

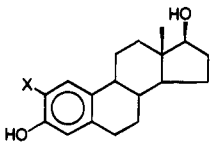

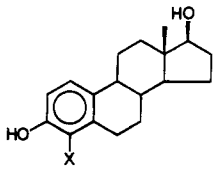

X		
Br	41	42
I	43	44

Figure 1. Forty-four substituted estradiol structures used to perform the QSAR/CoMFA.

chain orientation is determined by torsional angles (C-16,17,20,21) close to either −145° or −100° (anticlinal conformations). The energy of the molecules with a torsional angle of −100° is about 2−4 kcal/mol lower as compared to those with a −145° angle. The two sets of conformers (rotamers) were held in different databases to build separate QSAR tables, and the CoMF analyses were performed and compared (see below). The orientation of the 17β-OH group of our derivatives was characterized by a torsional angle of 72.1° (E_2), 62.0° (EE_2), and 54−55° (VE_2, 20*E*/*Z*-IVE_2). The 3-D spatial orientations of the bulky substituents on the 11β-position (OCH_3, OC_2H_5, and C_2H_5) of the various derivatives were also studied using a molecular mechanics approach (systematic search in the torsion angles space). No minimum energy conformations were found which differed significantly from those computed by MNDO, and therefore, the molecular structures were retained in the database as obtained from the MOPAC optimization.

In contrast to the relatively small conformational changes of the E_2 skeleton described above, the various substituents induced significant changes in the electron-charge distribution. This influenced the patterns of the isopotential surfaces surrounding the molecules and changed both the absolute value $|D|$ and the orientation of the molecular dipole (D_x, D_y, and D_z). Figure 4 shows

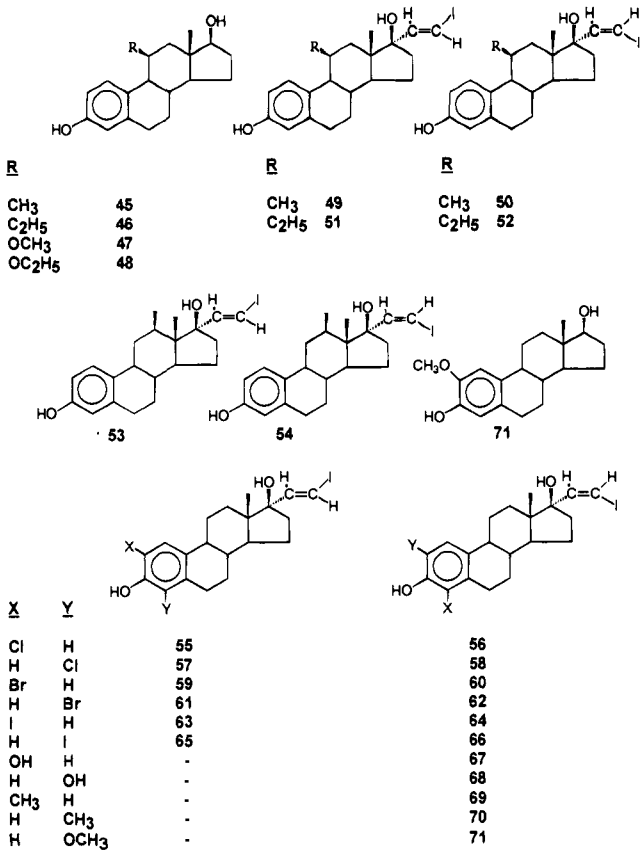

Figure 2. Structures of estradiol derivatives for which estrogen receptor-binding affinities were predicted from the QSAR/CoMFA model.

isopotential maps (±1.0 kcal/mol electrostatic potentials) of several model structures. The molecules were selected to exemplify the effect of electron-withdrawing and steric bulk atoms, i.e., at the 21-position (Cl and I) of the 17α-ethynyl and -vinyl group, the 11β-position (methoxy and ethoxy), and the 2(4)-positions (F), and of a neutral substituent (CH_3) at the 7α-position. The addition of a 17α-ethynyl group changes significantly the positive isopotential contour around estradiol and introduces a new electronegative region around the D-ring (Figure 4a). Introduction of the (20*E*)-iodovinyl group induces a similar effect, while in the case of the 20*Z*-isomer the positive isopotential surface shape seems less perturbed as compared to the parent molecule (Figure 4a). It is interesting to note that the presence of a 11β-OMe group influences the electronegative surface about the A-ring such that the resultant electronegative cavity, which originates from the 3-OH group, is extended toward and joined with the field of the 11β-OMe (Figure 4b). The field effect observed upon A-ring fluorination of the isomeric IVE_2 was similar to that observed for the analogous 16α-iodoestradiols.[7b] A substantial extension of the 3-OH electronegative cavity is observed when the 4-hydrogen is substituted by fluorine. A very different electronegative potential pattern is induced when the 2-hydrogen is substituted by fluorine. In the latter case, the enlarged electronegative cavity is divided by a protruding electropositive surface (Figure 4b). If partial atomic charges were computed using the Gasteiger–Hückel empirical method,[18] higher negative charges were assigned to the iodine atoms on the isomeric 17α(20*E*/*Z*)-iodovinyl derivatives and the 2(4)iodo-substituted estradiols (data not shown). In general however, as also observed by others,[14] QSAR/CoMFA results did not significantly depend on the method used for charge computation (see below).

QSAR and CoMF Analyses. Several QSAR tables were built with rows representing individual estradiol derivatives (from **1–40** to **1–44**, Figure 1). The first column of all QSAR tables incorporated experimental RBA ("explicit data", Tables 2 and 3), and all other columns were derived from CoMFA, except for QSAR run 3, which included four additional columns representing molecular dipoles (*x*-, *y*-, and *z*-components and absolute value of the total dipole, $|D|$). Because of the dependence of the relative interaction energies from molecular orientations in space, positioning molecular structures within a fixed lattice (molecular alignment) is the most important variable in CoMFA. Although in the study of Cramer et al.[1a] (see also SYBYL tutorial program[14b]) the "field-fit" minimization procedure is recommended as a molecular alignment rule, we found that the latter in our case did not give optimal cross-validation results (lower predictive r^2). This likely reflects the rigidity of the steroid skeleton, whose conformation is little affected by the different substituents. Among our trials, the best results were obtained using the rigid body rms fit of all skeleton carbon atoms of the A-, B-, and C-rings but omitting those of the D-ring (Figure 3). Attempts to keep steroid skeleton carbon atoms as constrains using restricted "field fit" in the presence of atomic aggregates were unsuccessful due to difficulties in achieving conversion criteria. Cramer and co-workers[1a] noted that changes in lattice spacing impacted on the output CoMFA results. Their cross-validated r^2 values indicated that a spacing of 2 Å between lattice points is a good choice for the steroid derivatives employed. In contrast, our trials showed that decreasing lattice spacing, e.g., from 2 to 1 Å, caused significant improvement of the CoMFA results, but this decrease required a 30–50-fold increase in the total computational time.

Table 1 summarizes results obtained from several CoMFA performed under different conditions (QSAR runs): rigid body A-ring carbon rms multifit (run 1); A-, B-, and C-ring carbon atom rms multifit (runs 2–7); full field fit (run 8); or field fit with A-, B-, and C-, and D-ring skeleton carbon atoms constrained as an aggregate (run 9). QSAR runs 6–14 differ from runs 1–5 in that the molecular database was constructed from 17α(20*E*/*Z*)-iodovinyl derivatives in which the torsional angle (C-16,17,20,21) was −100° (vs −145° in runs 1–5). The QSAR table (run 3) includes four additional columns consisting of molecular dipoles. CoMFA using steric or electrostatic fields only were also performed (runs 4 and 5, respectively). QSAR runs 10–14 were evaluated using a molecular database containing four additional molecules, e.g., **41–44** (Figure 1). Runs 11–14 differ from the other 10 in that the explicit data were introduced as ln(RBA). In most cases when the C atom was used as a probe, reasonably good CoMFA data vs RBA values were obtained with a cross-validated r^2 higher than ~0.6. In run 8, all molecules were aligned using field fit with subsequent MAXIMIN2 force field minimization. It is noteworthy, however, that the latter procedure strongly reduced the number of components required for optimal prediction, which obviously reflects

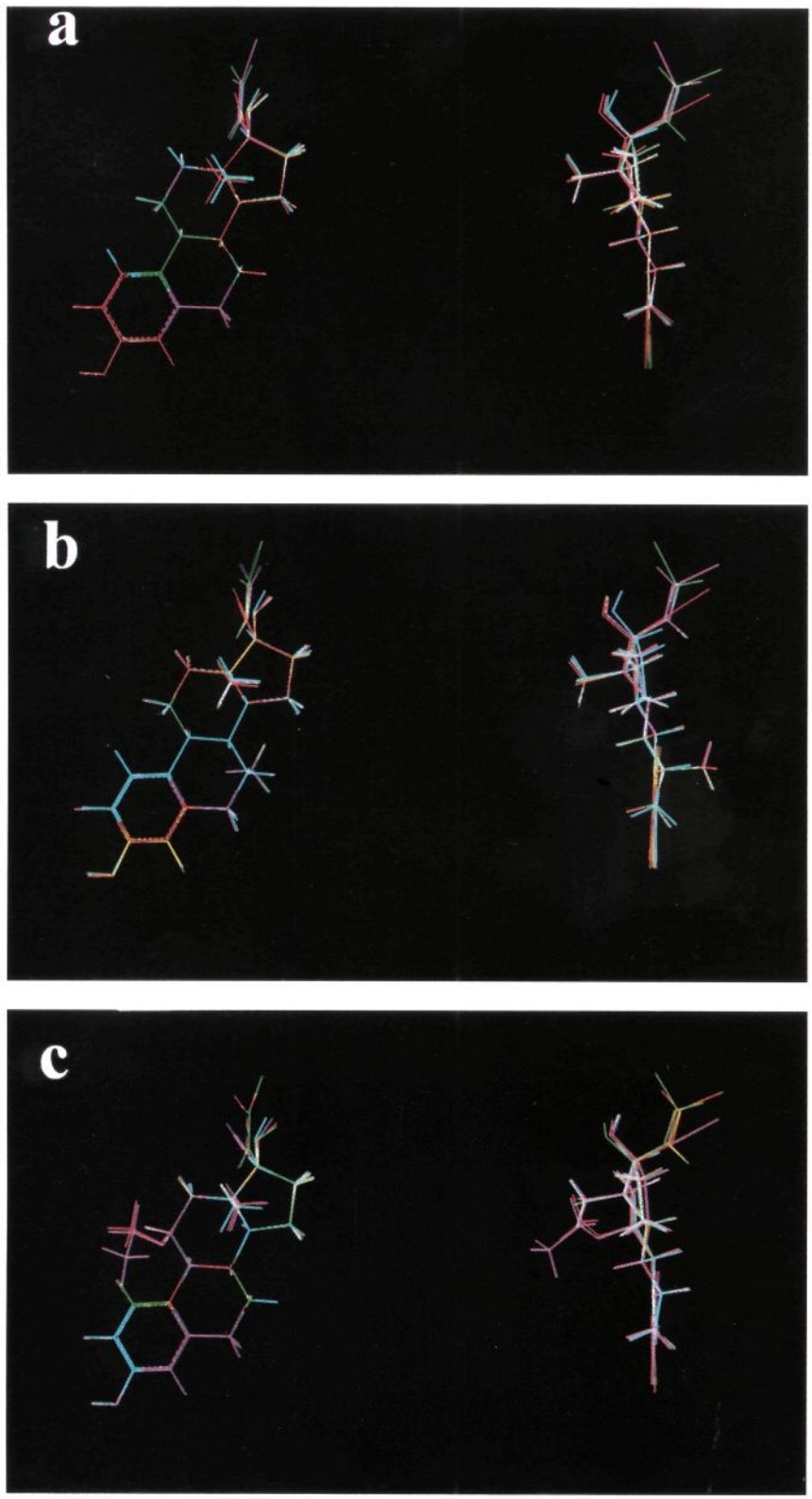

Figure 3. Orthographic stereoviews of overlapped 3-D structures (A-, B-, and C-ring rms fit) of estradiol derivatives: (a) template estrogen, E_2 (cyan), EE_2 (red), 20*E*-IVE_2 (green), and 20*Z*-IVE_2 (magenta); (b) E_2 (cyan), 2-F-7α-Me-EE_2 (red), 4-F-7α-Me-20*Z*-IVE_2 (green), and 2-F-7α-Me-20*E*-IVE_2 (magenta); and (c) E_2 (cyan), 11β-OMe-20*E*-IVE_2 (red), 11β-OMe-20*Z*-21-Cl-IVE_2 (green), and 11β-OEt-EE_2 (magenta).

the reduced complexity of the model. The introduction of molecular dipoles as additional independent columns in CoMFA (QSAR run 3) did not significantly improve the predictive power of the model. This is to be expected, since the dipoles of individual molecules depend on their 3-D electronic structures. If CoMFA was performed using steric or electrostatic fields independently, fields correlated somewhat better with experimental RBA (runs 3−5). In a separate database of 40 estradiol molecules, the partial atomic charges were

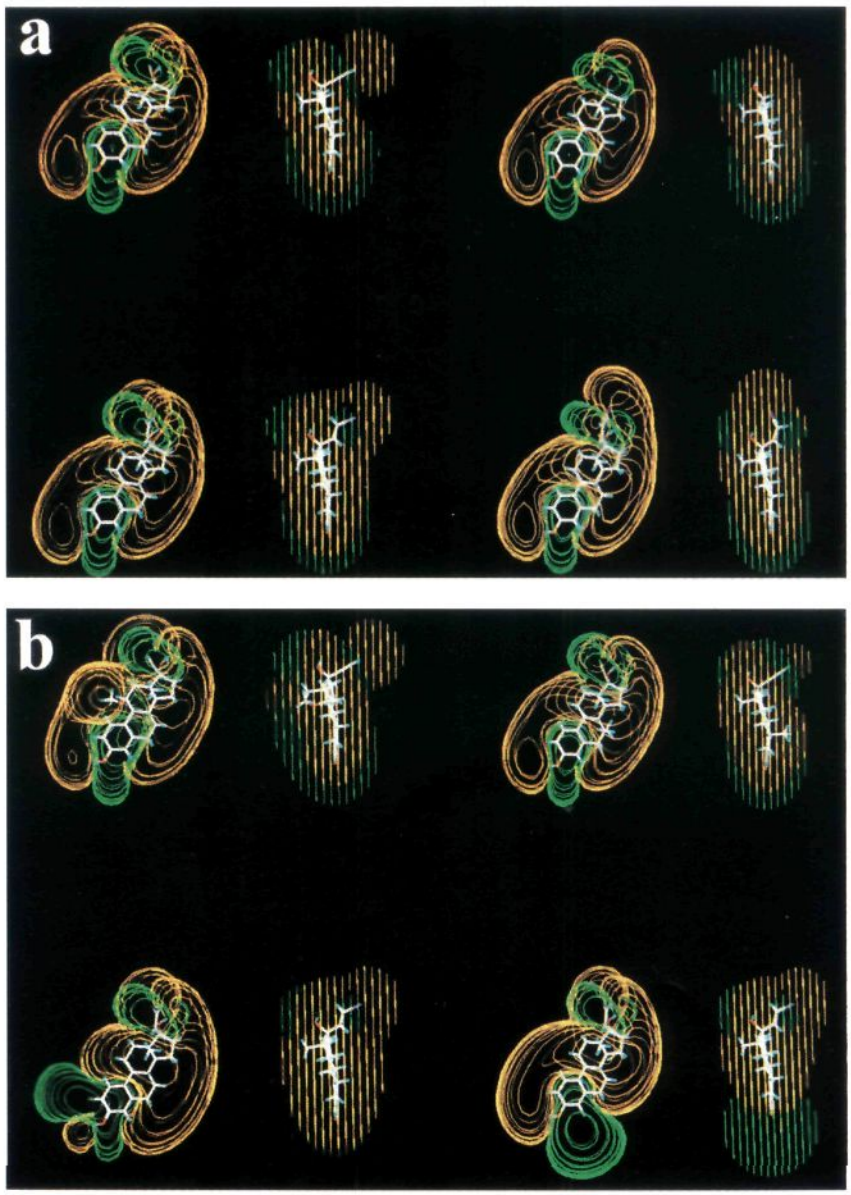

Figure 4. Orthographic stereoviews of electrostatic isopotential contours, 1.0 kcal/mol (yellow) and −1.0 kcal/mol (green): (a) E_2 (top right), EE_2 (top left), 20*E*-IVE_2 (bottom left), and 20*Z*-IVE_2 (bottom right) (b) 7α-Me-17α-Cl-EE_2 (top right), 11β-OMe-EE_2 (top left), 2-F-20*E*-IVE_2 (bottom left), and 4-F-20*E*-IVE_2 (bottom right).

also computed using the Gasteiger−Hückel method. After performing QSAR/CoMFA, using the same alignment rule (A-, B-, and C-ring rms fit; run 7), no marked improvement or distortion of the predictive/explanatory power of the model was obtained. This is in line with the known insensitivity of CoMFA to the method used for computing partial molecular charges.[14] The cross-validated analyses in the case of QSAR run 11 gave the highest $r^2 = 0.895$, and it was kept as the final output to predict receptor-binding properties of molecules which were not included in the database (see Figure 2). Typical CoMFA results (RBA from cross-validated and conventional PLS analyses) are presented in Table 2. Figures 5 and 6 show plots of the predicted vs actual binding affinities (RBA) and Qq-plots from the corresponding cross-validated and non-cross-validated CoMFA runs. A cross-validated $r^2 \simeq 0.9-1.0$ indicates excellent predictive ability of the model, and a conventional r^2 close to 1.0 is associated with excellent reproduction of the data used in the model derivation (data points in Figure 5 cluster around a line with a slope of 1). Although the plots shown in Figure 5 may mistakenly be interpreted as a two-point fit problem, our studies with different molecular subpopulations (e.g., omitting the four molecules, **41**−**44**, with ln(RBA) between −0.5 and 1.0) gave the same overall distribution pattern for the remaining 40 molecules. This is exemplified by the high observed r^2 (e.g., compare runs 6 and 10 in Table 1) with data points in the theoretical vs measured RBA well clustered around a line with a slope of 1. Molecules for which experimental binding values deviated strongly from the predicted RBA (QSAR run 11) are positioned at both ends of the Qq-plots, e.g., **5**, **6**, **8**, **22**, and **25** (Figure 6). The structures and alignments of these molecules were re-examined for conformity. Since the omission of the latter molecules from CoMF analyses did not improve substantially the predictive capacity (r^2), these molecules were retained in the model used for predicting unknown RBA.

Table 1. Selected Results of QSAR/CoMFA Studies with Different Input Variables, Alignment Rules, and Field Components (For structures of the estradiol derivatives **40–44**, see Figure 1)

					CoMFA					
						cross-validated			conventional	
QSAR run no.	compds	alignment rule	input variables	fields (steric and electrostatic)	groups	std error of predictions	optimal no. of components	r^2	std. error of estimate	r^2
1	**1–40**	A-ring rms fit	RBA	both	25	18.2	11	0.622	8.2	0.941
2	**1–40**	A,B,C-rings rms fit	RBA	both	40	17.3	10	0.652	7.4	0.936
3	**1–40**	A,B,C-rings rms fit	RBA $D(x,y,z)$[b]	both	40	19.1	20	0.694	2.8	0.994
4	**1–40**	A,B,C-rings rms fit	RBA	steric only	40	17.1	14	0.767	4.9	0.976
5	**1–40**	A,B,C-rings rms fit	RBA	electrostatic only	40	16.2	12	0.713	7.6	0.938
6	**1–40**[a]	A,B,C-rings rms fit	RBA	both	40	15.6	15	0.766	5.4	0.968
7	**1–40**[a]	A,B,C-rings rms fit	RBA	both[c]	20	15.4	14	0.759	2.4	0.984
8	**1–40**[a]	field fit (full)	RBA	both	40	19.7	3	0.566	14.2	0.710
9	**1–40**[a]	field fit (A,B,C,D-rings fixed)	RBA	both	40	17.2	11	0.667	5.5	0.965
10	**1–44**[a]	A,B,C-rings rms fit	RBA	both	44	21.4	16	0.693	4.3	0.982
11	**1–44**[a]	A,B,C-rings rms fit	ln(RBA)	both	25	0.475	11	0.895	0.158	0.988
12	**1–44**[a]	A,B,C-rings rms fit	ln(RBA)	both[d]	12	1.21	6	0.467	0.954	0.686
13	**1–44**[a]	A,B,C-rings rms fit	ln(RBA)	both[e]	25	1.20	3	0.462	0.935	0.591
14	**1–44**[a]	A,B,C-rings rms fit	ln(RBA)	both[f]	25	0.998	11	0.551	0.334	0.950

[a] Molecular database containing a different set of 17α-vinyl anticlinal oriented rotamers with a torsional angle (C-16,17,20,21) equal to −100°. [b] Total dipole and its *x*-, *y*-, and *z*-components. [c] Atomic charges computed by the Gasteiger–Hückel method. [d] Probe atom C (sp^3) with switching the dielectric function on atomic edges. [e] Probe atom O.3 (charge = −1) without switching the dielectric function. [f] Probe atom H (charge = 1) without switching the dielectric function. QSAR run 11 was preferred for prediction of unknown RBA. QSAR runs 1–11 were performed using a sp^3 carbon atom as a probe and a grid step of 1 Å without switching off the dielectric function.

The molecular fields in most of above CoMF analyses (runs 1–11) were probed using a sp^3 carbon atom with a formal charge of 1. The dielectric function was distance dependent (electrostatic energy, $E \simeq 1/r^2$) with an energy cutoff lacking a transition region. In a parallel set of molecular field evaluations, we also mapped steric and electrostatic interactions using different probe atoms. Additional variables were employed as follows: hydrogen and oxygen (O.3) probe atoms with formal charges of 1 and −1, respectively; change of dielectric function with a smooth transition between "the inside" and "the outside" of the atoms; and field averaging. These variables were particularly selected to probe the hydrogen-bonding (acceptor or donor) properties of the estradiols. The output from several additional analyses are listed in Table 1 (runs 12–14). In general, it can be noted that the substitution of the probe atom from a sp^3 carbon to hydrogen or oxygen resulted in a lower predictive capacity of the model (lower cross-validated r^2) while retaining good explanatory properties as confirmed by the non-cross-validated and "bootstrapping" computations. These evaluations were not applied for prediction purposes; instead they were used to visualize the regions where hydrogen-bonding interactions may be of importance. A series of computations were also performed using various subsets of the total database of 44 molecules in order to discriminate between different field regions of importance in the increase or decrease of the targeting properties. Subsets included selective omission of either the 17α(20*E*)- or 17α(20*Z*)-iodovinyl isomers or the 17α-ethynyl derivatives. The predictive power of these models were lower (r^2 = 0.4–0.5), and therefore they were not retained for other analysis.

CoMFA Coefficient Contour Maps. The QSAR produced by CoMFA is represented as a 3-D "coefficient contour map".[1a] The standard deviation/coefficient maps (STDEV*COEFF) derived from the final model after employing QSAR run 11 (sp^3; +1 carbon atom as a probe) are shown in Figure 7 (a, steric, and b, electrostatic fields). These contours display 3-D space areas, where small changes in molecular fields are strongly associated with changes of receptor-binding affinities. The interaction magnitudes are color-coded, and in the case of steric fields (Figure 7a), red and yellow contours surround regions where higher steric interference would increase binding affinity for ER and cyan and green contours indicate areas associated with undesirable steric interactions, i.e., where a decrease in steric interference would improve ER binding. To aid visualization, the van der Waals (vdW) radii of the various substituents, i.e., 21-I at 17α(20*E*/*Z*)-vinyl, H atoms of the 17α-ethynyl, 11β-OMe and 7α-Me, and H, F, and Cl atoms at 2- and/or 4-positions, are shown as colored dotted clouds (Figure 7). The model suggests a strong influence of the 17α(20*E*)-vinyl and 17α-ethynyl substituents (75–90% of total steric contributions) on receptor-binding properties. It can also be seen that the ER tolerates an increase of the steric bulk in the 17α-(20*Z*)-vinyl orientation. The interactions in the area occupied by substituents on the 17α-ethynyl or 17α-(20*E*)-vinyl groups are more complicated since steric bulk can contribute to increase the binding affinity, but only if the vdW radii stay within the 21-I vdW radii of the 17α(20*E*)-iodovinyl group. Two areas near C-15 and in the direction of the 17β-OH also are associated with better biological properties and most likely reflect small changes in the D-ring geometry and/or the orientation of 17β-OH group. The subtle displacement of the 18-methyl group on C-13, in the various estradiol derivatives, does not influence the steric interactions with the receptor. On the other hand, steric bulk with a vdW surface larger than that of 11β-OMe (e.g., ethoxy but not ethyl) diminishes the binding affinity (cyan and blue polyhedra). Finally, A-ring substitutions with a vdW surface larger than the vdW volume of chlorine also result in lower receptor-binding affinity.

In contrast to the QSAR/CoMFA model derived for testosterone and corticosteroids,[1a] our estradiol model bearing halogen substituents shows relatively high electrostatic contributions (normally 35–40% of total and for some molecules close to 70%) in the overall

Table 2. RBA Values as Obtained from the Final Cross-Validated and Non-cross-validated CoMFA for a Series of Estradiol Derivatives (QSAR/CoMFA run 11 in Table 1)

no.	estradiol derivatives	experimental RBA[a] (%)	predictions	
			cross-validated	non-cross-validated
1	estradiol (E_2)	100.0	84.1	99.0
2	ethynyl-E_2 (EE_2)	100.0	72.6	97.2
3	17α(20*E*)-iodovinyl-E_2 (20*E*-IVE_2)	39.7	30.2	35.1
4	17α(20*Z*)-iodovinyl-E_2 (20*Z*-IVE_2)	46.7	42.1	43.5
5	2-F-EE_2	64.3	21.5	42.7
6	2-F-20*E*-IVE_2	6.2	13.3	9.7
7	2-F-20*Z*-IVE_2	53.7	55.2	55.7
8	4-F-EE_2	119.0	177.0	161.3
9	4-F-20*E*-IVE_2	55.9	34.6	46.2
10	4-F-20*Z*-IVE_2	66.9	77.4	72.2
11	11β-OMe-EE_2	15.3	16.0	15.2
12	11β-OMe-20*E*-IVE_2	27.7	27.4	25.5
13	11β-OMe-20*Z*-IVE_2	32.0	29.6	29.5
14	2-F-11β-OMe-EE_2	15.9	19.4	15.5
15	2-F-11β-OMe-20*E*-IVE_2	13.5	13.4	14.8
16	2-F-11β-OMe-20*Z*-IVE_2	27.9	34.3	27.5
17	4-F-11β-OMe-EE_2	16.7	20.6	16.5
18	4-F-11β-OMe-20*E*-IVE_2	27.7	25.4	27.0
19	4-F-11β-OMe-20*Z*-IVE_2	37.9	34.2	39.5
20	11β-OEt-EE_2	21.0	16.9	22.1
21	11β-OEt-20*E*-IVE_2	17.1	19.9	18.2
22	7α-Me-EE_2	73.1	149.8	93.5
23	7α-Me-20*E*-IVE_2	43.2	41.7	40.8
24	7α-Me-20*Z*-IVE_2	44.9	58.0	50.2
25	2-F-7α-Me-EE_2	33.3	17.7	26.3
26	2-F-7α-Me-20*E*-IVE_2	12.1	13.6	13.5
27	2-F-7α-Me-20*Z*-IVE_2	28.6	21.8	27.4
28	4-F-7α-Me-EE_2	62.4	51.9	66.4
29	4-F-7α-Me-20*E*-IVE_2	36.4	23.6	28.9
30	4-F-7α-Me-20*Z*-IVE_2	36.8	36.3	34.8
31	17α-Cl-EE_2	53.4	33.2	51.4
32	17α(20*Z*)-21-Cl-IVE_2	49.4	53.6	50.7
33	11β-OMe-17α-Cl-EE_2	29.4	28.7	27.4
34	11β-OMe-17α(20*Z*)-21-Cl-IVE_2	35.0	41.9	34.8
35	11β-OEt-17α-Cl-EE_2	33.1	40.0	33.9
36	11β-OEt-17α(20*Z*)-21-Cl-IVE_2	31.7	27.5	31.1
37	7α-Me-17α-Cl-EE_2	37.6	43.7	40.3
38	7α-Me-17α(20*Z*)-21-Cl-IVE_2	36.8	33.4	36.6
39	2-F-17α-VE_2	17.6	11.1	18.5
40	4-F-17α-VE_2	73.7	68.8	70.7
41	2-Br-E_2	1.2	1.4	0.8
42	4-Br-E_2	5.0	1.7	1.1
43	2-I-E_2	0.4	1.0	0.6
44	4-I-E_2	0.1	0.7	0.6

[a] Maximum experimental errors of ±11.9% (**7**), ±11.7% (**8**), ±16.7% (**9**), and ±12.3% (**10**) and less for all other derivatives.

receptor interactions. The areas associated with the strongest electrostatic interactions are visualized on the electrostatic field coefficient map (Figure 7b). In the space delineated by the 17α-ethynyl (or -vinyl) group there is a small area (red and yellow), where increase of the negative charge should augment binding affinity, and a more distant area (green and cyan), where increase of the positive charge is recommended for increased binding affinity. In the space surrounding the A-ring, an increase in positive charge is advantageous for small substituents on C-2 while C-4 will tolerate larger positive groups for better binding affinity. On the other hand, in the area at the outer vdW radius of the 2-Cl (cyan), an increase of the negative charge is associated with higher binding affinity. No electrostatic influence from 11β-OMe (-OEt) substituents is recognized by this model. One important feature of both steric and electrostatic interaction field contours is their asymmetry in respect to the A-ring plane. Finally, it should be noted that other QSAR/CoMFA analyses performed with QSAR runs 1–10 (Table 1) gave rise to very similar field coefficient maps, with the only difference that models derived from runs 1–9 were not sensitive to steric bulks within the steroidal A-ring sphere. Similar graphic presentations of the steric field effects were obtained using a sp^3 carbon with a charge of 1 as a probe atom, with switching of the distance dependent dielectric function at the edges of the atomic radii, allowing a smoother field transition between the "inside" and "outside" of a given atom (QSAR run 12 in Table 1; graphic not shown).

To analyze hydrogen-bonding properties of the estradiol derivatives, we performed CoMFA by changing the probe atom from carbon to oxygen (O.3; formal charge = −1) or hydrogen (H; formal charge = 1) for hydrogen-bond donor or acceptor fields, respectively (QSAR runs 13 and 14). The steric field contributions (e.g., when C.3 or O.3 was used as the probe atom) did not differ significantly, but several important differences could be distinguished when electrostatic donor/acceptor fields were compared (Figures 8 and 9). Increasing the positive charge in the space surrounding the 17β-OH and 17α(20*Z*)-vinyl groups (yellow and red polyhedra) will favor H-bond donor interactions contributing to improve ER-binding properties. Increasing negative charges around the 17α-ethynyl and 17α(20*E*)-vinyl

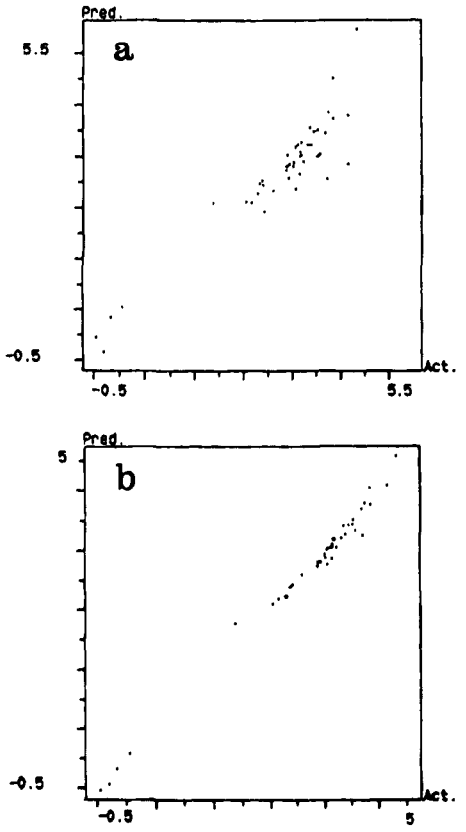

Figure 5. Relationships between predicted vs experimental ln(RBA) residuals for 44 estradiol derivatives as derived from final QSAR/CoMFA (Table 1, run 11): (a) cross-validated models and (b) non-cross-validated models (see also Table 2).

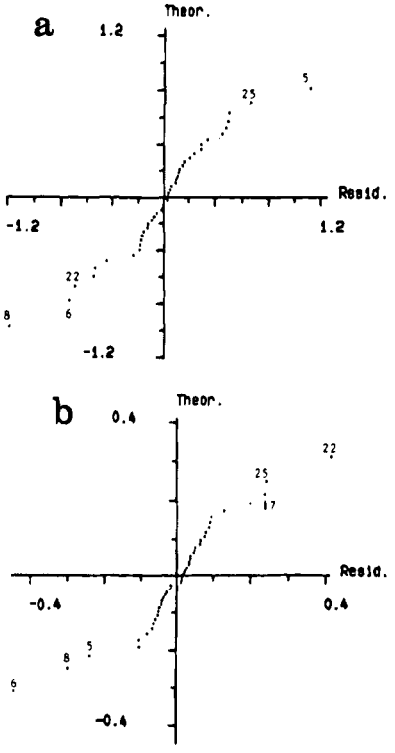

Figure 6. Qq-plots from final QSAR/CoMFA for 44 estradiol derivatives: (a) cross-validated models and (b) non-cross-validated models. Molecules for which large differences are obtained between experimental and predicted RBA are identified by number (Figure 1).

groups (white, cyan, and green area) also contribute to better target properties. The model also identifies asymmetric areas around the A-ring where changes in the partial charges influence H-bond donor interactions (Figure 8a). The relative contributions of the different regions to H-bonding and ER-binding properties are represented in Figure 8b. The region about the 17β-OH provides the highest contributions (90–100% and 50–75%) followed by the region around the 3-OH (C-4-substituents). 3-D space positions associated with the H-bond acceptor field (Figure 9) are complementary to the H-bond donor field, implying that an increase of positive charges nearby 17α-ethynyl and 17α(20*E*)-vinyl substituents improves ER binding. However, around the 17α(20*Z*)-vinyl group, an increase in positive charge is favored, in both the H-bond donor and acceptor fields. In the H-bond acceptor field, the influence of the 17β-OH group is diminished while the area about the 3-OH has become more important. Also in the H-bond acceptor field, our model predicts that an increase of the positive charge about 11β-substituents will augment ER-binding properties. Figure 9b shows the relative contributions to the H-bond acceptor field. The cyan area (0–25%), which covers almost the whole vdW estradiol envelope, indicates that the subtle changes at the estradiol periphery influence H-bond acceptor properties, with the strongest contributions (favorable or not) originating from the 17α-ethynyl group and the space surrounding the 3-OH followed by other areas occupied by 11β-, 2-, and 4-substituents.

Predictions. The resultant QSAR/CoMFA model (run 11) was used to predict the estrogen receptor-binding affinities of estradiol derivatives not included in the database (structures shown in Figure 2). Four 11β-substituted (Me, Et, OMe, and OEt) estradiols (**45**–**48**) and 11β-Et-17α(20*E*)-IVE_2 (**51**) represent a control group of compounds with known RBA values. Their predicted RBA are in very good agreement with experimental values. The remaining estradiol derivatives (Figure 2 and Table 3) were not previously reported, and their RBA values are unknown. From the calculated values, it follows that 11β-Me(Et)-17α(20*Z*)-IVE_2 (**50** and **52**) are the most promising iodinated derivatives in the series. The model predicts that addition of a 12β-Me group to IVE_2 results in a 2-fold lower RBA, as compared to **50** or **52**. Although the predictions for the A-ring (2- and 4-halogens)-substituted estradiols (**55**–**66**) show that these derivatives are not of practical importance (low RBA), the data illustrate to what extent steric and/or electron-withdrawing properties of the substituents interfere with receptor binding. While atoms and groups with a large vdW surface (I, Br, or CH_3) reduce the binding affinity very strongly, the more electronegative Cl atom (or F atom), particularly on C-4, can preserve to some degree the receptor-binding properties of the molecule. This is most likely due to favorable electrostatic interactions, contributing to the electrostatic field originating from the 3-OH group, as visualized by the electrostatic contours and coefficient maps (Figures 4, 7b, and 8, respectively). It is important to note, however, that substitution of OH for H at the 2- or 4-position (independently from favorable electrostatics at C-4) or substitution with large steric bulk (I, Br, or CH_3) groups results in low RBA, due to unfavorable steric interactions, as illustrated by field coefficient contours (Figure 7). In contrast, the predicted RBA value of 24.8 for the 2-methoxyestradiol[20]

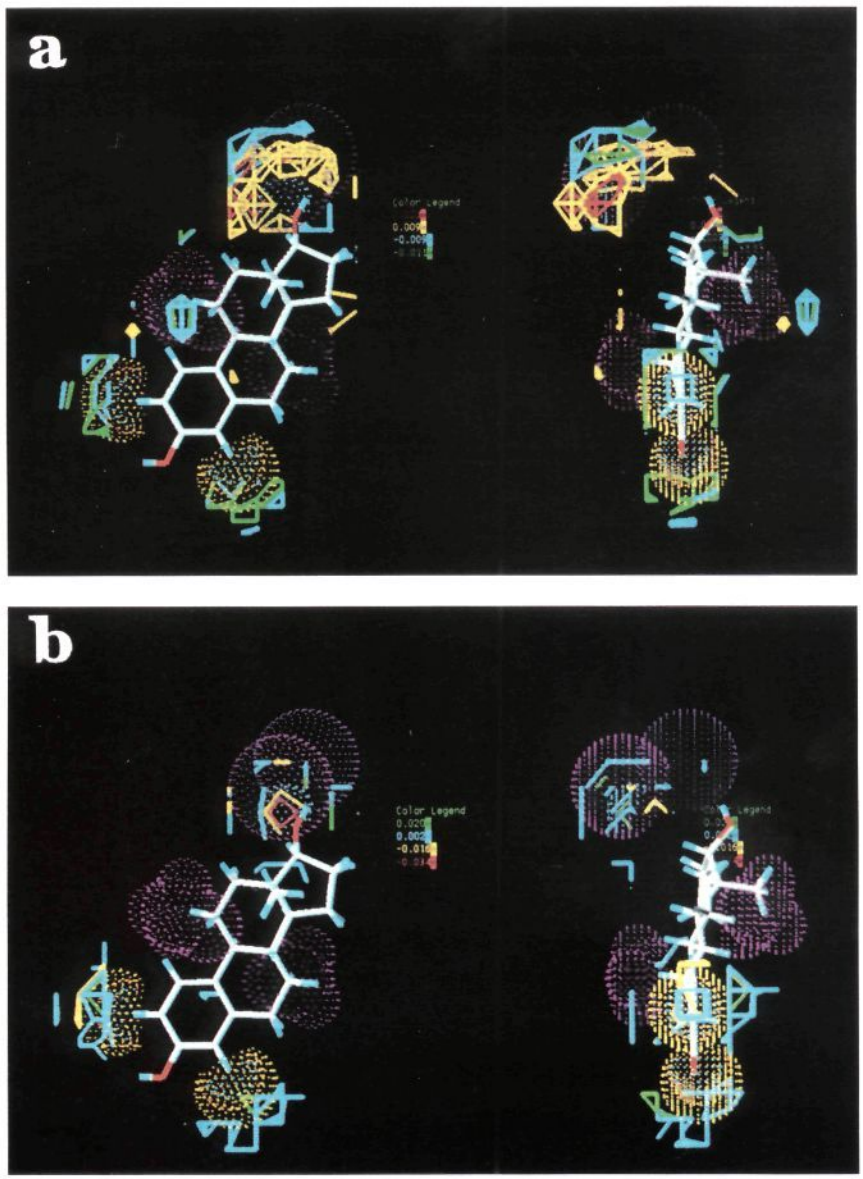

Figure 7. Orthographic stereoview of CoMFA steric field contours. The green and cyan polyhedra (STDEV*COEFF = −0.011 and −0.009, respectively) indicate regions where lower steric interaction would increase the binding affinity. The red and yellow contours (STDEV*COEFF = 0.020 and 0.009, respectively) surround regions where higher steric interactions would increase binding affinity. Dotted clouds represent vdW surfaces of the 21-iodine atoms with 20*E*- (magenta) and 20*Z*- (purple) configurations; H atom of 17α-ethynyl group (cyan); 7α-Me and 11β-OMe (magenta); 2(4)-H atoms (cyan); 2(4)-Cl atoms (yellow); and 2(4)-F atoms (orange). (b) Orthographic stereoview of CoMFA electrostatic field contours. The red and yellow contours (STDEV*COEFF = −0.034 and −0.016, respectively) indicate regions where addition of negative charge (decrease of positive charge) would increase binding affinity. Cyan and green contours (STDEV*COEFF = 0.002 and 0.020, respectively) indicate regions where addition of positive charge would increase the binding affinity. Dotted clouds represent vdW surfaces as indicated in (a). Data are from QSAR run 11.

(**71**) is notably higher than that of any other 2-substituted derivative of the series. This reflects most likely favorable electrostatic interactions arising from the negatively charged oxygen atom, in accordance with the graphics presentation of the field contours (Figures 7 and 8).

Discussion

CoMFA is a molecular conformation/configuration dependent 3-D QSAR technique, and therefore one of the most important input parameters is the alignment of the molecules within the region of the database where steric and electrostatic fields are sampled.[1,2] Variations in both the molecular superimposition and the conformational flexibility of molecules can influence the outcome from CoMFA. The results obtained with several different alignment rules for our training set of 40 estradiol derivatives are summarized in Table 1. It appears that the rms multifit procedure is the most appropriate alignment, in the case of the relatively rigid estradiol structures. This is in part a consequence of the fact that MNDO semiempirical computations represent a higher order geometry optimization technique as compared to molecular mechanics (Tripos MAXIMIN2) force field minimization following "field-fit" alignment. In fact, the latter alignment procedure resulted in significant distortions of the steroid skeleton. This is in line with the largely accepted preference of

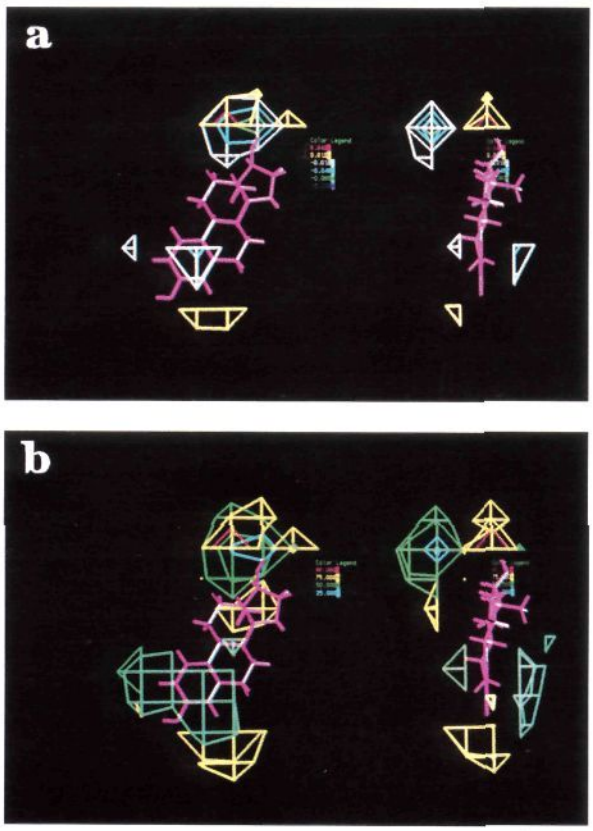

Figure 8. (a) Electrostatic field contours for hydrogen-bonding (donor) interactions. Output of actual STDEV*COEFF, values from QSAR/CoMFA run 13, Table 1; red- and yellow-colored polyhedra indicate regions where increased positive charge would provide for better target property; white, cyan, and green colors indicate regions where increased negative charge is recommended. (b) Same as in (a), but instead of actual values of STDEV*COEFF, the relative contributions were calculated; cyan (0–25%), green (25–50%), yellow (50–75%), and red (75–90%).

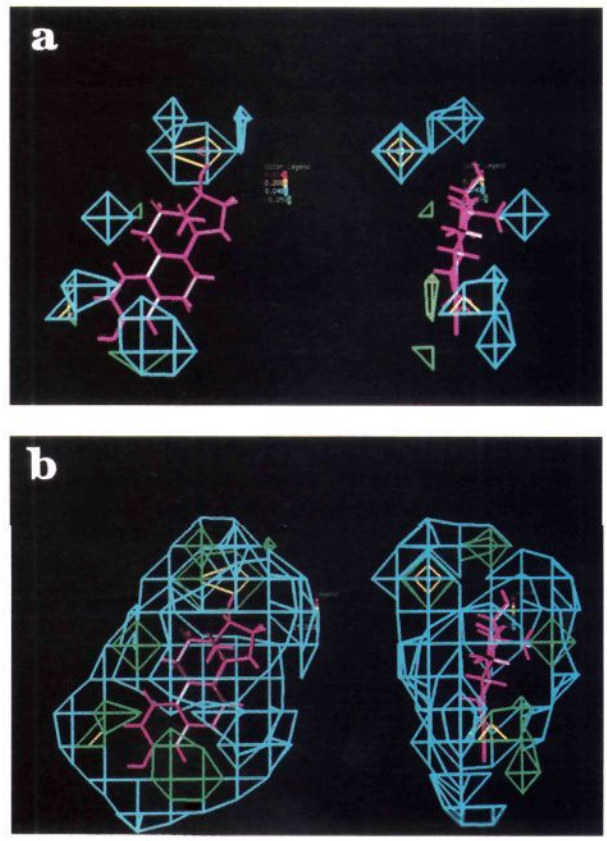

Figure 9. (a) Same as in Figure 8a but, instead, a plot of the hydrogen-bonding (acceptor) electrostatic field (output from QSAR/CoMFA run 14, Table 1). For better target property, increased positive charge is recommended in areas surrounded by red, yellow, and cyan polyhedra. Favorable increase of negative charge is indicated by green polyhedra. (b) Same as in (a), but relative contributions are plotted. Color legend is as in Figure 8b.

semiempirical computations (especially MNDO and AM1) to study the conformation of large organic type molecules.[21] However, "field-fit" alignment reduced significantly the complexity of our model, as exemplified by the reduced number of components required for its best statistical determination (Table 1), which, on the other hand, is the main advantage of CoMFA when applied to a molecular database containing highly flexible or conformationally diverse derivatives.

Regarding the conformational properties of the estradiol derivatives used to perform QSAR/CoMFA, it should be emphasized that the most useful parameter to select a biologically active conformation is the cross-validated r^2, the latter being a measure of how well predicted biological properties correspond to experimental values of the complete database. Due to the lack of other structural data, the orientations of substituents were kept as obtained from MNDO optimization. Our assumption that the minimum energy conformation is a good choice is confirmed by high r^2 values obtained throughout this study. For instance, we found that CoMFA using the anticlinal orientation of the 17α-vinyl group with the lower energy conformation results in a somewhat higher r^2 (Table 1). Other estradiol substituents for which minimum energy conformations were selected are the OC_2H_5, OCH_3, and C_2H_5 groups attached to the 11β-position.

Several CoMF analyses were performed using different probe atoms and dielectric functions. QSAR run 11 (Table 1), where molecular fields were probed with a sp^3 carbon atom with a distance dependent dielectric function, showed the highest r^2 and was used for the prediction of RBA of unknown analogs (Table 3). The H-bonding interactions were studied separately using oxygen and hydrogen as probe atoms. The results and electrostatic field contour maps (Figures 8 and 9) illustrate the hydrogen-bond donor/acceptor behavior of our model. For example, substituents on the D-ring influence more significantly hydrogen-bond donor (as compared to acceptor) functions of the 17α-OH group. In contrast, substituents on the C-2-position of the A-ring strongly influence the H-bond acceptor properties of the 3-OH group, while those at the 4-position perturb stronger the H-bond donor properties of this group.

It is well known that the 3-OH group in estradiol plays an anchor role in the receptor-binding process, and conformational changes within the region of the planar phenolic A-ring are not tolerated.[3a] At the same time, the receptor is also sensitive, albeit to a much lesser degree, to conformational changes of the D-ring induced by D-ring substituents. The rather accurate results (predictive r^2, Table 1) obtained when only the A-ring carbon atoms of the introduced molecules were rms fitted, as compared to A-, B-, and C-ring rms multifits, are likely associated with these properties of the ER.

Table 3. Predicted RBA Values for a Series of Estradiol Derivatives, Originally Not Included in the Database (From QSAR run 11 in Table 1)

no.	molecules	RBA predicted	RBA experimental
45	11β-Me-E_2	49.7	65[a]
46	11β-Et-E_2	58.3	78[a]
47	11β-OMe-E_2	15.6	7.0[a]
48	11β-OEt-E_2	13.5	10.0[a]
49	11β-Me-17α(20*E*)-IVE_2	45.2	–
50	11β-Me-17α(20*Z*)-IVE_2	55.7	–
51	11β-Et-17α(20*E*)-IVE_2	43.8	43.0[a]
52	11β-Et-17α(20*Z*)-IVE_2	54.1	–
53	12β-Me-17α(20*E*)-IVE_2	19.3	–
54	12β-Me-17α(20*Z*)-IVE_2	26.1	–
55	2-Cl-17α(20*E*)-IVE_2	7.1	–
56	2-Cl-17α(20*Z*)-IVE_2	10.7	–
57	4-Cl-17α(20*E*)-IVE_2	13.7	–
58	4-Cl-17α(20*Z*)-IVE_2	24.8	–
59	2-Br-17α(20*E*)-IVE_2	5.1	–
60	2-Br-17α(20*Z*)-IVE_2	8.3	–
61	4-Br-17α(20*E*)-IVE_2	6.4	–
62	4-Br-17α(20*Z*)-IVE_2	8.4	–
63	2-I-17α(20*E*)-IVE_2	3.5	–
64	2-I-17α(20*Z*)-IVE_2	5.4	–
65	4-I-17α(20*E*)-IVE_2	4.1	–
66	4-I-17α(20*Z*)-IVE_2	6.2	–
67	2-OH-17α(20*Z*)-IVE_2	14.5	–
68	4-OH-17α(20*Z*)-IVE_2	9.3	–
69	2-Me-17α(20*Z*)-IVE_2	7.4	–
70	4-Me-17α(20*Z*)-IVE_2	8.0	–
71	2-OMe-E_2	24.8	–

[a] Data from ref 13.

Further conformational/configurational diversity of the model, reflecting the complicated receptor interactions about the D-ring, follows from the CoMFA of 17α(20*E*/*Z*)-iodovinyl-substituted estradiols, implying that 20*Z*-positional isomers are better tolerated by the receptor than the 20*E*-positional isomers. Both steric and electrostatic interactions in this area are significant (Figure 7). At the same time, the derived models show little (or none) changes in estradiol–receptor steric interactions that can be associated with displacements of the 17β-OH group due to substituents at the 17α-position. The CoMFA analyses also imply that the presence of a 7α-Me group does not exert significant interactions in this region. Smaller bulk substituents onto the 11β-position (Me or OMe) did not influence sterically the predicted receptor-binding affinity, but longer chain groups (OEt) induced a decrease in binding affinity, as graphically exemplified in Figure 7. Rather surprisingly, alterations of the electrostatic field of estradiol resulting from the presence of the 11β-OMe (-OEt) substituents (Figure 4) did not exert any additional columbic interactions with the receptor (Figure 7b) but can participate in H-bond acceptor interactions (Figure 9). CoMFA indicates that both steric and electrostatic contributions (including H-bonding) arise from substituents on C-2 and C-4 of the A-ring. Bulky atoms (I and Br) at these positions, as a rule, are not tolerated by the receptor, but atoms with smaller vdW radii are acceptable (Figure 7a). Increasing the positive charge at C-4 is recommended, while contrasting electrostatic contributions toward C-2 are recognized (Figure 7b).

Evidence for the good performance of the QSAR/CoMFA derived model(s) is provided in Figures 5 and 6 which show plots of predicted vs experimental RBA residuals and the corresponding Qq-plots for cross-validated and conventional PLS runs. The average absolute residue values did not exceed 20–30% of the experimental RBA (see also Table 2), which is within the experimental error of such *in vitro* assays. Molecules for which significantly different RBA values were predicted include some of the ethynyl derivatives (e.g., **5**, **8**, **22**, and **25** in Table 2 and Figure 6).

To avoid fluctuations in RBA values due to different experimental conditions, most experimental values were taken from our own published data. In spite of differences in RBA measurements between laboratories (for example, EE_2 in our procedure gave RBA = 100 vs 75–220 as reported in the literature[13a,b,19]), the RBA predictions for five molecules which were not included in our model (**45–48** and **51**, Table 3) compare well with literature data. Thus, the predicted RBA for the test molecules, as summarized in Table 3, should have practical value. It is evident that RBA values alone are not sufficient to predict the nuclear imaging potential of the modified, radiolabeled steroids. Nonspecific binding, interaction with other steroid receptors, and metabolic rates are of equal importance in defining their capacity to accumulate in target organs. In this regard, our model complements QSAR/CoMFA models build for testosterone and corticosteroid,[1a] as well as those for progestin and androgen[1d] receptors. Receptor-binding affinity remains however the key event in predicting the potential of the drug for the receptor-mediated tissue localization process, and computer modeling appears to be a valid approach to predict essential structural features of candidate radiopharmaceuticals.

Acknowledgment. This work was supported by the Medical Research Council of Canada and the Ministère de l'Enseignement Supérieur et de la Science du Québec (Programme d'actions structurantes). The authors acknowledge the generous allocation of computer time by the Department of Chemistry of the Université de Sherbrooke and the technical assistance of M. Drouin.

References

(1) (a) Cramer, R. D., III; Patterson, D. E.; Bunce, J. D. Comparative molecular field analysis (CoMFA). 1. Effect of shape on binding of steroids to carrier proteins. *J. Am. Chem. Soc.* **1988**, *110*, 5959–5967. (b) Marshall, G. R.; Cramer, R. D., III. Three-dimensional structure-activity relationships. *Trends Pharmacol. Sci.* **1988**, *9*, 285–289. (c) Clark, M.; Cramer, R. D., III; Jones, D. M.; Patterson, D. E.; Simeroth, P. E. Comparative molecular field analysis (CoMFA). 2. Toward its use with 3D-structural databases. *Tetrahedron Comput. Methodol.* **1990**, *3*, 47–59. (d) Loughney, D. A.; Schwender, C. F. A comparison of progestin and androgen receptor binding using the CoMFA technique. *J. Comput.-Aided Mol. Des.* **1992**, *6*, 569–581.

(2) (a) Waller, C. L.; Oprea, T. I.; Giolitti, A.; Marshall, G. R. Three-dimensional QSAR of human immunodeficiency virus (I) protease inhibitors. 1. A CoMFA study employing experimentally-determined alignment rules. *J. Med. Chem.* **1993**, *36*, 4152–4160. (b) Waller, C. L.; Marshall, G. R. Three-dimensional quantitative structure-activity relationship of angiotensin-converting enzyme and thermolysin inhibitors. II. A comparison of CoMFA models incorporating molecular orbital fields and desolvation free energies based on active-analog and complementary-receptor-field alignment rules. *J. Med. Chem.* **1993**, *36*, 2390–2403. (c) DePriest, S. A.; Mayer, D.; Naylor, C. B.; Marshall, G. R. 3D-QSAR of angiotensin-converting enzyme and thermolysin inhibitors: a comparison of CoMFA models based on deduced and experimentally determined active site geometries. *J. Am. Chem. Soc.* **1993**, *115*, 5372–5384. (d) Agarwal, A.; Pearson, P. P.; Taylor, E. W.; Li, H. B.; Dahlgren, T.; Herslöf, M.; Yang, Y.; Lamber, G.; Nelson, D. L.; Regan, J. W.; Martin, A. R. Three-dimensional quantitative structure-activity relationships of 5-HT receptor binding data for tetrahydropyridinylindole derivatives; a comparison of the Hansch and CoMFA methods.

J. Med. Chem. **1993**, *36*, 4006–4014. (e) Diana, G. D.; Kowalczyk, P.; Treasurywala, A. M.; Oglesby, R. C.; Pevear, D. C.; Dutko, F. J. CoMFA analysis of the interactions of antipicornavirus compounds in the binding pocket of human rhinovirus-14. *J. Med. Chem.* **1992**, *35*, 1002–1008.

(3) (a) Counsell, R. E.; Klausmeier, W. H. Radiotracer interactions with sex steroid hormone receptor proteins (receptor mapping). In *Principles of Radiopharmacology*; Colombetti, L. G.; Ed.; CRC Press: Boca Raton, FL, 1979; Vol. II, pp 59–91. (b) Eckelman, W C.; Reba, R. C. Labeled estrogens and analogues. In *Radiopharmaceuticals: Structure-Activity Relationships*; Spencer, R. P., Ed.; Grune and Stratton: New York, 1981; pp 449–458. (c) Katzenellenbogen, J. A. The pharmacology of steroid radiopharmaceuticals: specific and non-specific binding and uptake selectivity. In *Radiopharmaceuticals Chemistry and Pharmacology*; Nunn, A. D., Ed.; Marcel Dekker: New York, 1992; pp 297–331. (d) Cummins, C. H. Radiolabeled steroidal estrogens in Cancer Research. *Steroids* **1993**, *58*, 245–259.

(4) (a) Hochberg, R. B. Iodine-125-labeled estradiol: a gamma emitting analog of estradiol that binds to the estrogen receptor. *Science* **1979**, *205*, 1138–1140. (b) Zielinski, J. E.; Yabuki, H.; Pahuja, S. L.; Larner, J. M.; Hochberg, R. B. 16α-[^{125}I]Iodo-11β-methoxy-17β-estradiol: a radiochemical probe for estrogen-sensitive tissues. *Endocrinology* **1986**, *119*, 130–139. (c) Zielinski, J. E.; Larner, J. M.; Hoffer, P. B.; Hochberg, R. B. The synthesis of 11β-methoxy-[16α-^{123}I]iodoestradiol and its interaction with the estrogen receptor in vivo and in vitro. *J. Nucl. Med.* **1989**, *30*, 209–215. (d) Ali, H.; Rousseau, J.; van Lier, J. E. 7α-Methyl- and 11β-ethoxy-substitution of [^{125}I]-16α-iodoestradiol: effect on estrogen receptor-mediated target tissue uptake. *J. Med. Chem.* **1993**, *36*, 264–271.

(5) (a) Ali, H.; Rousseau, J.; Ghaffari, M. A.; van Lier, J. E. Synthesis, receptor binding and tissue distribution of (17α,20E)- and (17α,20Z)-21-[^{125}I]iodo-19-norpregna-1,3,5(10),20-tetraene-3,17-diol. *J. Med. Chem.* **1988**, *31*, 1946–1950. (b) Ali, H.; Rousseau, J.; Ghaffari, M. A.; van Lier, J. E. *Synthesis*, receptor binding, and tissue distribution of 7α- and 11β-substituted (17α,-20E)- and (17α,20Z)-21-[^{125}I]iodo-19-norpregna-1,3,5(10),20-tetraene-3,17-diols. *J. Med. Chem.* **1991**, *34*, 854–860. (c) Jagoda, E. M.; Gibson, R. E.; Goodgold, H.; Ferreira, N.; Francis, B. E.; Reba, R. C.; Rzeszotarski, W. J.; Eckelman, W. C. [I-125]17α-iodovinyl 11β-methoxyestradiol: in vivo and in vitro properties of a high-affinity estrogen-receptor radiopharmaceutical. *J. Nucl. Med.* **1984**, *25*, 472–477. (d) Nakatsuka, I.; Ferreira, N. L.; Eckelman, W. C.; Francis, B. E.; Rzeszotarski, W. J.; Gibson, R. E.; Jagoda, E. M.; Reba, R. C. Synthesis and evaluation of (17α,20E)-21-[^{125}I]iodo-19-norpregna-1,3,5(10),20-tetraene-3,17-diol and (17α,20E)-21-[^{125}I]iodo-11β-methoxy-19-norpregna-1,3,5-(10),20-tetraene-3,17-diol(17α-[iodovinyl]estradiol derivatives) as high specific activity potential radiopharmaceuticals. *J. Med. Chem.* **1984**, *27*, 1287–1291. (e) McManaway, M. E.; Jagoda, E. M.; Kasid, A.; Eckelman, W. C.; Francis, B. E.; Larson, S. M.; Gibson, R. E.; Reba, R. C.; Lippman, M. E. [^{125}I]17-α-Iodovinyl 11-β-Methoxyestradiol interaction *in vivo* with estrogen receptors in hormone-independent MCF-7 human breast cancer transfected with the V-ras^{H} oncogene. *Cancer Res.* **1987**, *47*, 2945–2949. (f) Hanson, R. N.; Franke, L. A.; Kaplan, M. Radioiodinated ligands for the estrogen receptor: Tissue distribution of 17α-[^{125}I]Iodovinyl estradiol derivatives in normal and tumor-bearing adult female rats. *Nucl. Med. Biol.* **1990**, *17*, 239–245. (g) Merrick, M. V.; Corrie, J. E. T.; Millar, A. M.; Hawkins, R. A. A reevaluation of an agent proposed for imaging oestrogen receptors: 17α-[^{125}I]iodovinyl-11β-methoxyoestradiol-3-methyl ether ([^{125}I]VMEME). *Nucl. Med. Biol.* **1988**, *15*, 327–332. (h) Hanson, R. N.; Franke, L. A.; Kaplan, M. L. Synthesis and evaluation of (17α,20E)21-[^{125}I]Iodo-11-substituted-19-norpregna 1,3,5(10),20-tetraene-3,17β-diols: the influence of 11-stereochemistry on tissue distribution of radioiodinated estrogens. *Nucl. Med. Biol.* **1989**, *16*, 3–9. (i) Foulon, C.; Guilloteau, D.; Baulieu, J. L.; Ribeiro-Barras, M. J.; Desplanches, G.; Frangin, Y.; Besnard, J. C.; Estrogen receptor imaging with 17α-[^{123}I]Iodovinyl-11β-methoxyestradiol (MIVE$_2$) - Part I. Radiotracer preparation and characterization. *Nucl. Med. Biol.* **1992**, *19*, 257–261. (j) Ribeiro-Barras, M. J.; Foulon, C.; Baulieu, J. L.; Guilloteau, D.; Bougnoux, P.; Lansac, J.; Besnard, J. C.; Estrogen receptor imaging with 17α-[^{123}I]Iodovinyl-11β-methoxy estradiol (MIVE$_2$) - Part II. Preliminary results in patients with breast carcinoma. *Nucl. Med. Biol.* **1992**, *19*, 263–267.

(6) Hanson, R. N. The influence of structure modification on the metabolic transformation of radiolabeled estrogen derivatives. In *The chemistry and pharmacology of radiopharmaceuticals*; Nunn, A. D., Ed.; Marcel Dekker: New York, 1992; pp 333–364.

(7) (a) Ali, H.; Rousseau, J.; van Lier, J. E. Synthesis of A-ring fluorinated derivatives of (17α,20E/Z)-[^{125}I]iodovinyl estradiols: Effect on receptor binding and receptor-mediated target tissue uptake. *J. Med. Chem.* **1993**, *36*, 3061–3072. (b) Ali, H.; Rousseau, J.; Gantchev, T. G.; van Lier, J. E. 2- and 4-Fluorinated 16α-[^{125}I]iodoestradiol derivatives: *Synthesis* and effect on estrogen receptor binding and receptor-mediated target tissue uptake. *J. Med. Chem.* **1993**, *36*, 4255–4263.

(8) Raynaud, J. P.; Ojasoo, T. Receptor binding as a tool in the development of selective new bioactive steroids and non steroids. In *Innovative Approaches in Drug Research*; Harms, A. F., Ed.; Elsevier Science: Amsterdam, 1986; pp 47–72.

(9) (a) Raynaud, J. P.; Ojasoo, T.; Bouton, M. M.; Brignon, E.; Pons, M.; Crastes de Paulet, A. In *Estrogens in the Environment*; McLachlan, J. A., Ed.; Elsevier Science: New York, 1985; pp 24–42. (b) Kalvoda, von J.; Krähenbühl, Ch.; Desaulles, P. A.; Anner, G. A. 7α-Methylöstrogene. *Helv. Chim. Acta* **1967**, *50*, 281–288.

(10) Ali, H.; Rousseau, J.; van Lier, J. E. Synthesis, receptor binding and biodistribution of the Gem-21-chloro-21-iodovinylestradiol derivatives. *J. Steroid Biochem. Mol. Biol.* **1993**, *46*, 613–622.

(11) Schneider, W.; Shyamala, G. Glucocorticoid receptors in primary culture of mouse mammary epithelial cells: characterization and modulation by prolactin and cortisol. *Endocrinology* **1982**, *116*, 2656–2662.

(12) Heiman, D. F.; Senderoff, S. G.; Katzenellenbogen, J. A.; Neeley, R. J. Estrogen receptor based imaging agents. 1. Synthesis and receptor binding affinity of some aromatic and D-ring halogenated estrogens. *J. Med. Chem.* **1980**, *23*, 994–1002.

(13) (a) Liu, A.; Carlson, K. E.; Kazenellenbogen, J. A.; vanBrocklin, H. F.; Mathias, C. J.; Welch, M. J. Androgen receptor-based imaging agents for the prostate: synthesis and tissue distribution studies with tritium and fluorine-18 labeled androgens. *J. Labelled Compd. Radiopharm.* **1991**, *30*, 434–436. (b) Teutsch, G.; Ojasoo, T.; Raynaud, J. P. 11β-substituted steroids, an original pathway to antihormones. *J. Steroid Biochem.* **1988**, *31*, 549–565. (c) Zeelen, F. J.; Bergink, E. W. Structure-activity relationships of steroid estrogens. In *Cytotoxic Estrogenes in Hormone Receptive Tumors*; Raus, J., Martens, H., Leclercq, G., Eds.; Academic Press: New York, 1980; pp 39–48.

(14) (a) Tripos Associates, 1699 S. Hanley Rd., Suite 303, St. Louis, MO 63144. (b) SYBYL Tutorial Manual, Tripos Assoc.

(15) Cambridge Crystallographic Database, University Chemical Laboratory, Lensfield Rd., Cambridge CB2 1EW, U.K.

(16) Stewart, J. J. MOPAC: A general molecular orbital package (version 6.0). *Quantum Chemistry Program Exchange Catalogue* **1992**, *IV*, 19–20.

(17) Mulliken, R. S. Electronic population analysis on LCAO-MO molecular wave functions I. *J. Chem. Phys.* **1955**, *23*, 1833–1840.

(18) Gasteiger, J.; Marsili, M. Interactive partial equalization of orbital electronegativity - a rapid access to atomic charges. *Tetrahedron* **1980**, *36*, 3219–3288.

(19) Poirier, D.; Labrie, C.; Mérand, Y.; Labrie, F. Derivatives of ethynylestradiol with oxygenated 17α-alkyl side chain: synthesis and biological activity. *J. Steroid Biochem.* **1990**, *36*, 133–142.

(20) Hu-Ming, H.; Cushman, M. A versatile synthesis of a new anticancer metabolite, 2-methoxyestradiol. 208th ACS National Meeting (Division of Medicinal Chemistry), Washington, DC, 1994; p 80, Abstract.

(21) Suckling, C. J. Use and limitations of models and modelling in medicinal chemistry. In *Comprehensive Medicinal Chemistry*; Hansch, C., Sammes, P. G., Taylor, J. B., Eds.; Pergamon Press: New York, 1990; Vol. 4, pp 83–138.